Journal of Alloys and Compounds 777 (2019) 1030–1038

Contents lists available at ScienceDirect

Journal of Alloys and Compounds

journal homepage: http://www.elsevier.com/locate/jalcom

Enhanced room-temperature magnetocaloric effect and tunable magnetic response in Ga-and Ge-substituted $AlFe_2B_2$

R. Barua [a, b, *], B.T. Lejeune [a], B.A. Jensen [c], L. Ke [c], R.W. McCallum [d], M.J. Kramer [c], L.H. Lewis [a, e, **]

[a] Department of Chemical Engineering, Northeastern University, Boston, MA, United States
[b] Department of Mechanical & Nuclear Engineering, Virginia Commonwealth University, Richmond, VA, United States
[c] Division of Materials Science & Engineering, The Ames Laboratory, Ames, IA, United States
[d] McCallum Consulting LLC, Santa Fe, NM, United States
[e] Department of Mechanical and Industrial Engineering, Northeastern University, Boston, MA, United States

ARTICLE INFO

Article history:
Received 9 June 2018
Received in revised form
9 October 2018
Accepted 16 October 2018
Available online 21 October 2018

Keywords:
$AlFe_2B_2$
Magnetocaloric
Magnetic refrigeration
Thermal management

ABSTRACT

It is demonstrated that alloying additions of Ga and Ge enable tuning of the magnetocaloric response of the intermetallic boride $AlFe_2B_2$. Samples of nominal chemical composition $Al_{1.2-x}M_xFe_2B_2$ (M = Ga, Ge; $x \leq 0.30$) were synthesized via suction casting (arc-melting and vacuum drawing into cylindrical copper molds) and subsequent heat treatment (annealed to 1373 K for 72 h). The saturation magnetization (M_s), Curie temperature (T_c) and specific heat capacity (C_p) of the samples all increase with increased Ga and/or Ge additions. Relative to the unmodified parent $AlFe_2B_2$ compound, a larger than two-fold improvement in the magnetic entropy change (ΔS ($\mu_0 H_{app} = 2$ T) = 6.5 J kg^{-1}K^{-1}) and adiabatic temperature change (ΔT_{ad} ($\mu_0 H_{app} = 2$ T) = 2.2 K) was observed at 305 K in a sample of composition $Al_{1.1}Ga_{0.05}Ge_{0.05}Fe_2B_2$. The enhanced magnetocaloric response of the $Al_{1.2-x}(Ga,Ge)_xFe_2B_2$ system is ascribed to a complex amalgamation of chemical bonding and electronic effects that arise due to Fe and Al antisite defects within the $AlFe_2B_2$ lattice. Overall, these results provide insight of both fundamental and applied relevance concerning pathways for maximizing the magnetocaloric potential of $AlFe_2B_2$ for potential energy-related applications near room temperature.

1. Introduction

The magnetocaloric effect (MCE) is characterized by an isothermal entropy change (ΔS_{mag}) and an adiabatic temperature change (ΔT_{ad}) in a magnetic material arising from application and removal of a magnetic field [1]. This magneto-thermodynamic phenomenon forms the basis of many emerging technologies in the power and energy sector, including solid-state cooling, gas liquefaction, and thermal energy harvesting [2,3. Additionally, recent reports indicate that MCE systems may be potentially useful for biomedical applications such as magnetic resonance imaging (MRI), hyperthermia-based cancer treatment and magnetic nanoparticle-based drug delivery [4–6]. Each application demands materials with different properties, including range of operating temperatures, mechanical properties, thermal properties, and magnetic field sensitivities. Over the last 25 years, several materials that demonstrate an appreciable room-temperature MCE have been reported, including Gd, $Gd_5Si_2Ge_2$, FeRh, $La(Fe,Si)_{13}$-based compounds and their corresponding hydrides, MnFe(P,Ge,Si,As)-based pnictides and the NiMn-based Heusler alloys [7–12]. More recently, the intermetallic boride $AlFe_2B_2$ has attracted considerable attention for use in magnetic refrigeration technology due to its low cost, ease of manufacturing, promising magnetocaloric effect, tunable magnetic transition near room temperature, good mechanical stability and a low heat capacity that fosters effective heat transfer [13–15].

The $AlFe_2B_2$ compound adopts the orthorhombic Mn_2AlB_2-type (*Cmmm*) crystal structure, also referred to as the 1-2-2 structure, with a unit cell that contains two formula units (lattice parameters, a = 2.9233 Å, b = 11.0337 Å and c = 2.8703 Å).16 Within each formula unit, the Fe atoms are bonded to four equidistant neighboring

* Corresponding author. Department of Chemical Engineering, Northeastern University, Boston, MA, United States.
** Corresponding author. Department of Chemical Engineering, Northeastern University, Boston, MA, United States.
E-mail addresses: rbarua@vcu.edu (R. Barua), lhlewis@northeastern.edu (L.H. Lewis).

https://doi.org/10.1016/j.jallcom.2018.10.206
0925-8388/

B atoms (interatomic distance of 2.156 Å) and to a further two B atoms (with equal interatomic distances of 2.165 Å), Fig. 1. Such an arrangement can be envisioned as Fe_2B_2 layers of thickness 1.64 Å that are separated at a distance of 3.22 Å by a layer of Al atoms along the *b*-axis. The pseudo-binary Al-FeB phase diagram indicates that $AlFe_2B_2$ is formed by a peritectic reaction between the corresponding liquid and FeB at approximately 1553 K [14]. It is therefore difficult to synthesize single-phase $AlFe_2B_2$ by directly melting Al, Fe and B in the stochiometric 1:2:2 ratio. Undesirable secondary phases obtained during solidification (mainly $Al_{13}Fe_4$ and FeB) contribute to the magnetization of these alloys making evaluation of the inherent magnetofunctional response complicated [17].

The compound $AlFe_2B_2$ is ferromagnetic and upon heating it undergoes a ferromagnetic (FM) to paramagnetic (PM) Curie transition T_c near room temperature (measured T_c values for the unmodified composition are between 282 K and 320 K) with reported magnetic moments in the range 0.95–1.32 μB/Fe-atom [10–18]. In the vicinity of the T_c, magnetic entropy change ΔS_{mag} values ranging from 2.1 to 4.4 J kg^{-1}K^{-1} at $\mu_0 H_{app} = 2$ T have been reported in polycrystalline specimens of uncertain isotropy. Appreciable coupling is observed between the crystallographic and magnetic aspects of $AlFe_2B_2$. For example, the magnetic transition is accompanied by clear but subtle changes in the lattice parameters but produce only negligible change in the unit cell volume as noted in temperature-dependent X-ray and neutron diffraction data [12,15]. In agreement with experimental results [15,19], *ab initio* calculations reveal that the magnetic moments in the $AlFe_2B_2$ structure are oriented along the crystallographic *a*-axis.20 The *a*- and *c*-axes of $AlFe_2B_2$ are identified as the easy and hard axes of magnetization respectively with an in-plane anisotropy energy of K~1 MJ/m^3 [21]. The sizeable magnetocrystalline anisotropy in $AlFe_2B_2$ is accompanied by a significant room-temperature anisotropic magnetocaloric effect corresponding to a large rotating magnetic entropy change of 1.3 J kg^{-1}K^{-1} at $\mu_0 H_{app} = 2$ T when the spin quantization vector is rotated from the hard *c*-axis to the easy *a*-axis direction [21].

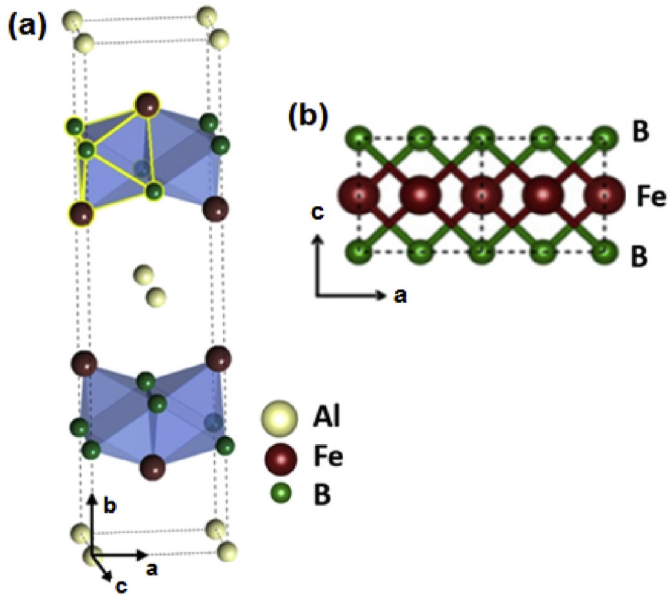

Fig. 1. Schematic representation of the orthorhombic crystal structure of $AlFe_2B_2$ from two perspectives: (a) Viewed along the b-axis, each unit cell consists of two formula units with Fe and B atoms forming chains of FeB polyhedra within the (ac) plane. Each slab is separated by a monolayer of Al atoms; (b) Top-view of the *ac*-plane indicates that the Fe_2B_2 chains form a wavy layer with Fe atoms located between parallel layers of B atoms.

To date, little work has been performed to clarify the effect of elemental substitution on the magnetocaloric response of $AlFe_2B_2$. A handful of reports have investigated the phase stability and magnetofunctional behavior of compositional variants of $AlFe_2B_2$, with most studies focused on compositions where Fe in the lattice is substituted by other *3d* transition-metal elements [22–25]. While $AlCo_2B_2$ and $AlNi_2B_2$ do not form under equilibrium conditions, the compounds $AlCr_2B_2$ and $AlMn_2B_2$ adopt the same *Cmmm*-type orthorhombic crystal structure as $AlFe_2B_2$ [24]. Additions of Mn and/or Co to $AlFe_2B_2$ decrease the magnetization, the T_c and the associated MCE [22,23,25]. The measured magnetic entropy change curves, as derived from application of the Maxwell Relations to magnetic data, of both $Al(Fe_{1-x}Co_x)_2B_2$ ($x \leq 0.0625$) and $Al(Fe_{1-x}Mn_x)_2B_2$ ($x = 0.1$) are reported to be broad, spanning a temperature range of 60–80 K [18,19]. Computational studies conducted by Kadas et al. and Ke et al. predict that alloying additions of transition and main group elements such as Cr, Ni, Be, Mg, Ga and C will change the magnetofunctional effect observed in this system [20,24]

Continuing the investigation of elemental incorporation into the $AlFe_2B_2$ lattice, in this work the impact on the structural and magnetic properties of $AlFe_2B_2$ from additions of Ga and Ge are reported. It is demonstrated that the magnetocaloric response of $AlFe_2B_2$ may be tuned over a temperature span of 50 K (260 K–310 K) by very small but systematic additions of Ga and Ge to the alloy. Relative to the unmodified parent compound, a significant improvement in the MCE response is noted in alloys of nominal composition $Al_{1.2-x}(Ga,Ge)_xFe_2B_2$ ($0 < x \leq 0.1$). Experimental data reported here indicate that the solid solubility of Ga and Ge in the $AlFe_2B_2$ lattice is very small; it is hypothesized that the presence of the substituent elements in the precursor alloy alters the solidification route for formation of the $AlFe_2B_2$ phase. Overall, the enhanced magnetocaloric response of $AlFe_2B_2$ compound modified with Ga and Ge is attributed to a combination of extrinsic (solidification pathway) and intrinsic (antisite occupancy) factors.

2. Experimental methods

Samples of nominal composition $Al_{1.2-x}M_xFe_2B_2$ wherein M = Ga and/or Ge, $0 < x < 0.3$, were synthesized from elemental granules (99.95% or higher) by arc-melting in an argon atmosphere. Arc-melting was repeated thrice to improve chemical homogeneity. As per guidance obtained from the pseudo-binary FeB-Al phase diagram [17], excess Al was added to the base compositions to maximize the $AlFe_2B_2$ phase content and reduce formation of detrimental boride phases after heat treatment. The arc-melted ingots were subsequently re-melted and suction-cast into a 5-mm cylindrical copper mold with average length of 4 cm. The suction-cast rods were then wrapped with tantalum foil and sealed in quartz ampoules backfilled with a partial pressure of ultra-high purity argon for annealing (heating rate of 10 K per minute) at 1313 K for 72 h. After furnace cooling to room temperature, the rods were sliced into multiple sections along the length of the ingot for investigation with a variety of thermal, structural and magnetic probes. Complete details regarding the sample synthesis procedure are available in Reference [14].

Room-temperature X-ray diffraction (XRD) data were measured using a Bruker diffractometer with a Cu-Kα radiation source to allow determination of lattice parameters and phase purity employing the Rietveld refinement feature in the program GSAS [26]. Specimens were mounted in resin and polished to a mirror finish using polishing paper (grits 400, 600, and 800) and diamond polishing paste (6 and 1 microns). The microstructures and average composition of these prepared samples were examined using field-

emission scanning electron microscopy (SEM, FEI Teneo, $V_{accel} = 20$ kV; I = 0.8 nA) and energy-dispersive spectroscopy (EDS, Oxford Aztec system with X-Max 80 detector). The multi-phase character of the as-cast samples were probed using differential scanning calorimetry (DSC) (Netzsch STA 409 PC) at a heating rate of 20 K/min in pure argon. The peritectic temperature was determined as the extrapolated onset of the first endothermic peak appearing in the DSC signal during heating. Magnetic characterization was carried out using Vibrating Sample Magnetometry (Quantum Design PPMS DynaCool and VersaLab models) in magnetic fields up to μ0Happ = 9 T in the temperature range 50 K ≤ T ≤ 400 K. For magnetic characterization, samples were cut into elongated shapes with their long axis oriented parallel to the applied magnetic field, and no demagnetization corrections were applied. To minimize instrumental errors related to thermal equilibrium and heat transfer, the magnetothermal temperature sweep-rate was set at 2 K/min. The Curie temperature T_c was determined from the inflection point of the *M vs. T* curve as the maximum of the derivative of *M* with respect to *T* (*i.e.* $\frac{\partial M}{\partial T}$). For $T > T_c$ the samples were confirmed to follow the Curie-Weiss law, $\chi = \frac{C}{T-\theta}$, where *C* is the Curie constant and θ is the paramagnetic Curie temperature. The effective moment (μ_{eff}) per Fe atom of the samples was estimated from the Curie constant (*C*) using the expression below:

$$C = \frac{N\mu_{eff}{}^2}{3Ak} \tag{1}$$

Here *N* is the number of magnetic atoms per mole of sample, *A* is the molecular weight and *k* is Boltzman's constant.

The magnetocaloric behavior of $AlFe_2B_2$ in the magnetic field range 0.5 < μ0Happ <2 T was quantified indirectly from magnetic entropy change curves (ΔS_{mag} *vs. T*) constructed by applying Maxwell's relation [Eq. (1)] to data obtained from isothermal *M*(*H*) curves measured at 2.5 K temperature intervals in the vicinity of the Curie temperature [1]:

$$\Delta S_{mag}(H,T) = \mu_0 \int_0^{H_{max}} \left(\frac{\partial M}{\partial T}\right)_H dH \tag{2}$$

Here, μ_0 is the permeability of free space, $\frac{\partial M}{\partial T}$ is the temperature derivative of the magnetization and H_{max} is the maximum applied field. The working temperature range (δT_{FWHM}) of the magnetocaloric samples was calculated as the difference between the extreme temperature ends of the full-width at half-maximum of the peak of the ΔS_{mag} vs. *T* curve. The temperature dependence of the entropy change in the absence of a magnetic field Δ*S*(*0,T*) was calculated from heat capacity data obtained using a heat-pulse calorimeter (Quantum Design PPMS System):

$$\Delta S(0,T) = \mu_0 \int_0^T \left(\frac{C_p}{T}\right) dT \tag{3}$$

Finally, the adiabatic temperature changes (ΔT_{ad}) of the samples were quantified as the isoentropic difference between two Δ*S*(*H,T*) curves measured at constant magnetic fields.

$$\Delta S(H,\ T) = \Delta S_{mag}(H,T) - \Delta S(0,T) \tag{4}$$

3. Experimental results

The impact of Ga- and Ge-additions on the microstructural features, crystallographic properties and magnetofunctional response of the intermetallic boride $AlFe_2B_2$ is presented in this section. The structural, magnetic and thermal attributes of the annealed $Al_{1.2-x}(Ga,Ge)_xFe_2B_2$ (x < 0.3) samples are described first; the magnetocaloric properties of the corresponding samples are described thereafter.

3.1. Chemical and structural attributes

The Rietveld-refined XRD pattern of the ternary sample of an initial chemical composition $Al_{1.2}Fe_2B_2$, Fig. 2, confirms attainment of a single-phase compound with the *Cmmm*-type orthorhombic crystal structure (lattice parameters: $a = 2.924(1)$ Å, $b = 11.029(9)$ Å, $c = 2.866(0)$ Å; unit cell volume: 92.42 Å^3). Fig. 3 shows changes in the lattice parameters and unit cell volumes of the Ga- and Ge-containing $Al_{1.2-x}(Ga,Ge)_xFe_2B_2$ samples relative to that of the undoped ternary sample. It is observed that all three lattice parameters and the corresponding unit cell volume increases

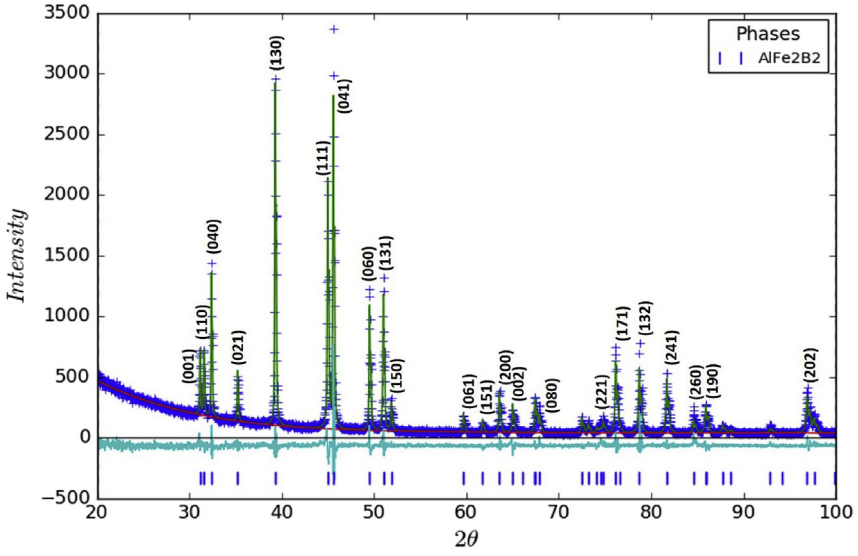

Fig. 2. XRD pattern of annealed $Al_{1.2}Fe_2B_2$ sample showing representative diffraction peaks which only correspond to the $AlFe_2B_2$ phase.

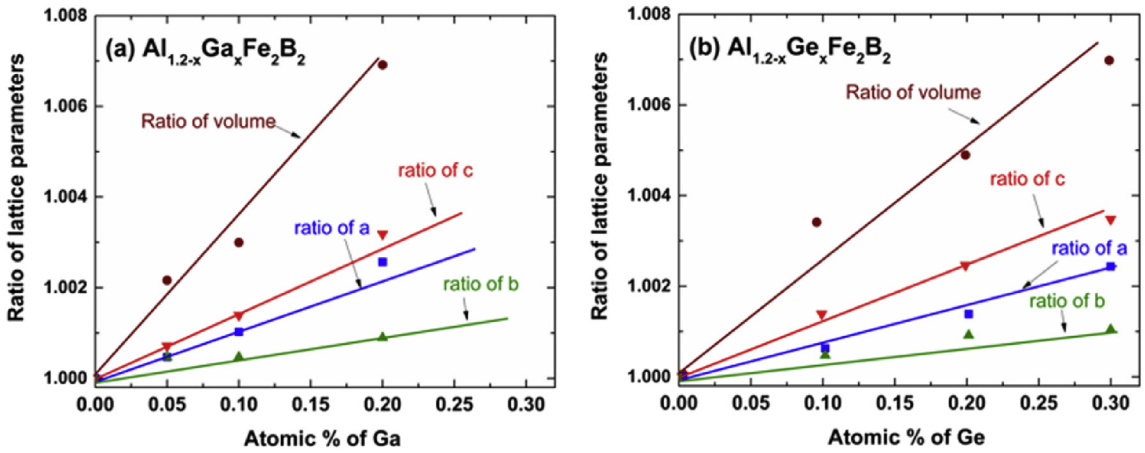

Fig. 3. Monotonic increase in unit cell volume and lattice parameters with increase in atomic % of Ga and Ge in samples of nominal composition, $Al_{1.2-x}M_xFe_2B_2$ (M = Ga and/or Ge; x < 0.3). The y-axis shows ratio between the lattice parameter of the compositional variant and the unmodified parent sample.

monotonically with increase in Ga and/or Ge (x) content. The change in the individual crystallographic axes due to Ga and Ge addition is anisotropic in character, such that increase in the *a*- and *c*-axes (up to 0.35% and 0.27%, respectively) is more significant than along the corresponding *b*-axis (only up to 0.11%), Fig. 3. While samples of nominal compositions $Al_{1.2-x}M_xFe_2B_2$ (M = Ga and/or Ge, $x \leq 0.1$) were confirmed to be single-phase within the detection limits of laboratory XRD, additional secondary phases (up to 15 wt % of FeB and 2 wt % of elemental Ge) were observed in lower Al content samples of nominal composition $Al_{1.0}Ga_{0.2}Fe_2B_2$, $Al_{1.0}Ge_{0.2}Fe_2B_2$ and $Al_{0.9}Ge_{0.3}Fe_2B_2$. Therefore the microstructure and average elemental chemical composition of only the single-phase $Al_{1.2-x}(Ga/Ge)_xFe_2B_2$ ($x \leq 0.1$) samples as determined by XRD were examined.

Fig. 4 shows representative SEM micrographs of annealed samples of nominal compositions $Al_{1.2}Fe_2B_2$ and $Al_{1.1}(Ge/Ga)_{0.1}Fe_2B_2$. While the annealed unmodified parent $Al_{1.2}Fe_2B_2$ sample is large-grained and chemically homogeneous (Fig. 4(a)), the microstructure of the annealed Ga- and Ge-containing compositional variants were found to be highly porous (Fig. 4(b) and (c)). Quantification of Fe and Al content using EDS reveals that the Fe:Al atomic ratio within the $AlFe_2B_2$ phase increases from 1.96 to 2.04 as the atomic % of Ga and Ge increases from 0 to 0.1, Fig. 5. Despite the realization that EDS does not typically allow a reliable estimation of boron, these measured values were found to be qualitatively close to the expected boron content value of 40 at.%. Intriguingly, negligible Ga and Ge (<0.2 at%) was detected by EDS in all the annealed single-phase samples.

The crystallographic properties (lattice parameters, unit cell volume), phase purity and Fe:Al atomic ratio of the $Al_{1.2-x}M_xFe_2B_2$ (M = Ga and/or Ge, $x \leq 0.1$) samples are summarized in Table 1. As the fraction of Ga and Ge within the $AlFe_2B_2$ grains in the annealed samples was found to be small (less than 10 at% of the amount added to the original starting composition), the Fe:Al atomic ratio in the $AlFe_2B_2$ phase may be considered as a reliable indicator of the compositional evolution within the annealed samples. Relative to the unmodified parent sample, an overall increase in the lattice parameters and the unit cell volume with an increase in Fe:Al ratio is observed in the annealed single-phase $Al_{1.2-x}M_xFe_2B_2$ samples, Fig. 6.

3.2. Thermal attributes & phase evolution

Calorimetric data obtained upon heating the annealed $Al_{1.2-x}(Ga,Ge)_xFe_2B_2$ ($x \leq 0.1$) samples in the temperature range

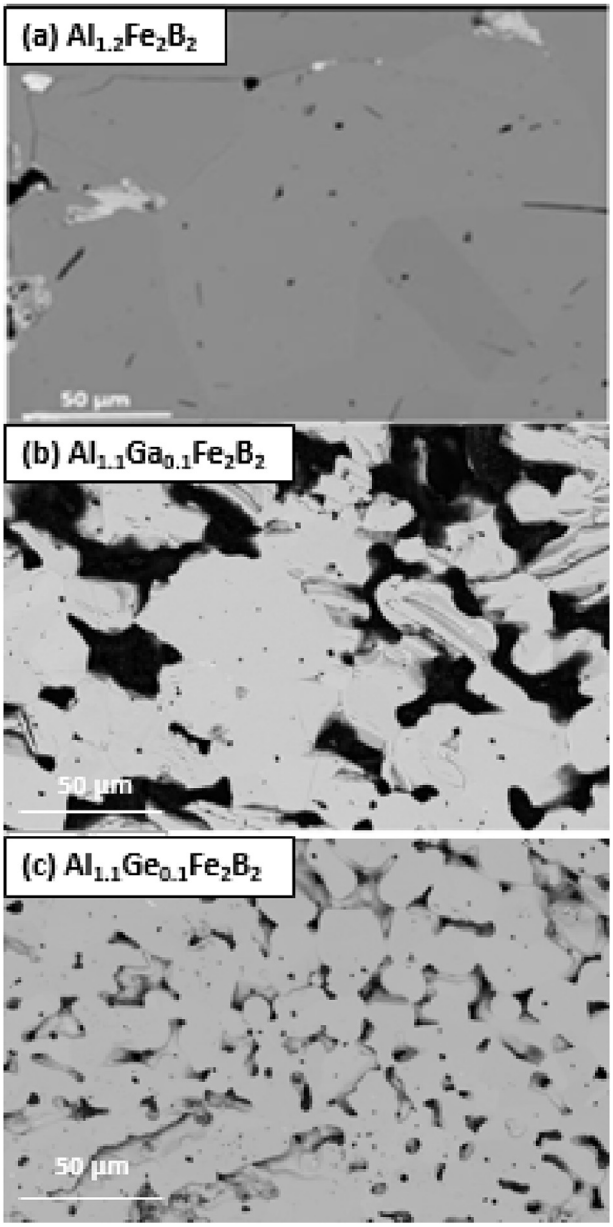

Fig. 4. SEM micrographs of annealed samples of nominal composition, $Al_{1.2}Fe_2B_2$, $Al_{1.1}Ge_{0.1}Fe_2B_2$ and $Al_{1.1}Ga_{0.1}Fe_2B_2$.

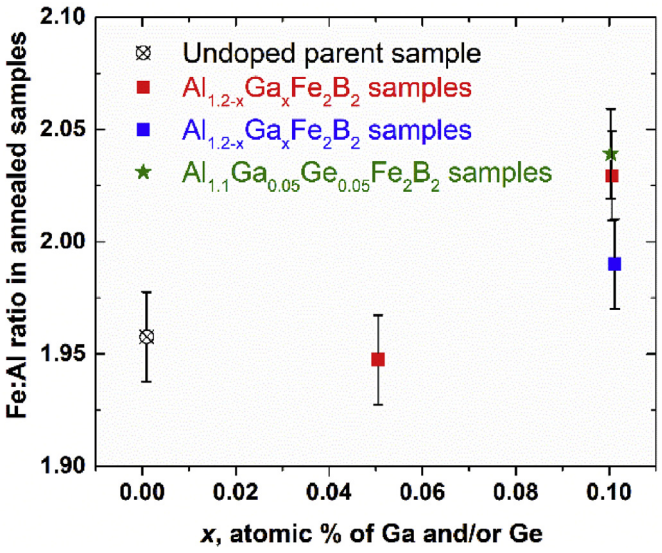

Fig. 5. Relationship between atomic% (x) of Ga and Ge in samples of nominal composition $Al_{1.2-x}(Ga,Ge)_xFe_2B_2$ and the Fe:Al atomic ratio of the $AlFe_2B_2$ phase in the annealed samples.

300 K < T < 1773 K, shown in Fig. 7(a), indicate that the parent $Al_{1.2}Fe_2B_2$ sample demonstrates an endothermic peak associated with the peritectic decomposition reaction of the $AlFe_2B_2$ phase into FeB and the corresponding liquid upon heating to 1551 K. Additions of Ga and Ge decreases the peritectic temperature (T_p) to a minimum of 1511 K in the sample of composition $Al_{1.0}Ga_{0.2}Fe_2B_2$. Systematic trends were observed in the relationship between T_{peri} and the composition of the samples, such that T_p decreases monotonically with increased Ga and Ge content in the $Al_{1.2-x}(Ga,Ge)_xFe_2B_2$ samples, Fig. 7(b).

3.3. Magnetic attributes

Temperature-dependent magnetization curves measured at an applied magnetic field of 20 kOe ($\mu_0 H_{app} = 2$ T) and field-dependent magnetic measurements at 50 K are provided in the Supplementary Section. The parent $Al_{1.2}Fe_2B_2$ sample exhibits a Curie temperature at $T_c = 272$ K with M_s (50 K) = 78 emu/g. Samples of composition $Al_{1.2-x}(Ga,Ge)_xFe_2B_2$ ($x < 0.2$) are completely paramagnetic for $T > T_c$ (insets of Figs. S1(b) and S2(b) of the Supplementary Section). The ferromagnetic signal detected for $T > T_c$ in the lower Al-content samples ($Al_{1.0}Ga_{0.2}Fe_2B_2$, $Al_{1.0}Ge_{0.2}Fe_2B_2$ and $Al_{0.9}Ge_{0.3}Fe_2B_2$) is attributed to the presence of FeB, in agreement with the XRD data (see Table 1). Relative to the unmodified sample, nominally single-phase samples of starting composition $Al_{1.2-x}(Ga,Ge)_xFe_2B_2$ ($x < 0.2$) demonstrate an increase in M_s and T_c with increase in Ga and/or Ge additions, Fig. 8. A maximum value corresponding to $T_c = 294$ K and M_s (50 K) = 86 emu/g was noted in the annealed $Al_{1.1}Ge_{0.05}Ga_{0.05}Fe_2B_2$ specimen. The magnetic properties of the annealed Ga- and Ge-substituted $AlFe_2B_2$ samples are summarized in Table 2.

3.4. Magnetocaloric response

Magnetic entropy change curves (ΔSmag vs. T plots) measured at μ_0Happ = 2 T from the samples of this study are shown in Fig. 9(a). The parent $Al_{1.2}Fe_2B_2$ sample demonstrates a broad magnetic entropy change curve with a working temperature range $\delta T_{FWHM} = 24$ K (spanning the temperature range 262 K–286 K) and a peak magnetic entropy change corresponding to $\Delta S_{mag}^{peak} = 2.7$ J kg^{-1}K^{-1} at T = 274 K. The zero-field heat capacity value of the sample $Al_{1.2}Fe_2B_2$ was determined as $C_p = 123$ J/mole·K and, employing Eqs. (3) and (4), the associated adiabatic temperature change of this compositionally unmodified sample was estimated as ΔT_{ad}~1 K at $\mu_0 H_{app} = 2$ T, Fig. 9(b). Additions of Ga and Ge donate an increase in the C_p, ΔS_{mag}^{peak} and ΔT_{ad} values and decrease the δT_{FWHM}, (Table 3 and Fig. 9). Significantly, a larger than two-fold enhancement in the MCE was measured in the $Al_{1.1}Ge_{0.05}Ga_{0.05}Fe_2B_2$ specimen ($\Delta S_{mag} = 6.5$ J kg^{-1}K^{-1}, ΔT_{ad} ~ 2.4 K at $\mu_0 H_{app} = 2$ T). The magnetocaloric properties of the single-phase samples of composition $Al_{1.2-x}(Ga,Ge)_xFe_2B_2$ ($x < 0.2$) are summarized in Table 3.

4. Discussion

All experimental data reported here indicate that the phase stability, magnetic properties and magnetocaloric response of $AlFe_2B_2$ may be significantly modified by very slight alloying additions of Ga and Ge. The lattice parameters of the unmodified parent $AlFe_2B_2$ phase, which are consistent with previous reports [10–13], are systematically increased with Ga and Ge additions (see Table 1 and Fig. 3). The solid-solubility concentrations of Ga and Ge within the $AlFe_2B_2$ lattice are confirmed to be very small, as incorporation of the dopant elements to the $Al_{1.2-x}(Ga,Ge)_xFe_2B_2$ starting composition for $x \geq 0.2$) leads to the formation of secondary phases, mainly FeB (Table 1). Further, less than 10% of the nominal amount of Ga and/or Ge initially added to the samples is detected within the $AlFe_2B_2$ grains of the annealed samples. Considering that the melting temperatures of Al ($T_m = 932$ K) and of the dopant elements Ga ($T_m = 307$ K) and Ge ($T_m = 1211$ K) are much lower than that of Fe ($T_m = 1811$ K) and B ($T_m = 2349$ K), it is likely that segregation of Ga and Ge to the Al-rich peritectic liquid occurs during the synthesis process. This inference is supported by the observation that the microstructure of the unmodified parent $Al_{1.2}Fe_2B_2$ sample is large-grained and chemically homogeneous while that of the annealed $Al_{1.1}Ga_{0.1}Fe_2B_2$ and $Al_{1.1}Ge_{0.1}Fe_2B_2$ samples is very porous, Fig. 4.

Though the peritectic temperature (T_p) of the $Al_{1.2-}$

Table 1
Crystallographic properties of annealed samples of nominal composition $Al_{1.2-x}M_xFe_2B_2$ (M = Ga or Ge, $0 < x \leq 0.30$).

General chemical composition	*a*-parameter (Å)/% increase relative to $Al_{1.2}Fe_2B_2$	*b*-parameter (Å)/% increase relative to $Al_{1.2}Fe_2B_2$	*c*-parameter (Å)/% increase relative to $Al_{1.2}Fe_2B_2$	Volume (Å^3)	wt.% $AlFe_2B_2$ phase	Fe: Al atomic ratios in single phase $AlFe_2B_2$ samples
$Al_{1.2}Fe_2B_2$	2.924(1)	11.029(9)	2.866(0)	92.42	100	1.95
$Al_{1.15}Ga_{0.05}Fe_2B_2$	2.926(7)/+0.07	11.034(2)/+ 0.04	2.868(5)/+0.07	92.63	100	1.94
$Al_{1.1}Ga_{0.1}Fe_2B_2$	2.927(2)/+0.10	11.035(1)/+0.05	2.870(2)/+0.14	92.72	100	2.04
$Al_{1.0}Ga_{0.2}Fe_2B_2$	2.932(0)/+0.27	11.039 (8)/+ 0.09	2.875/+0.31	93.06	99; 1 wt% FeB	–
$Al_{1.1}Ge_{0.1}Fe_2B_2$	2.928(4)/+0.07	11.036(9)/+0.06	2.870(0)/+0.14	92.75	100	2.00
$Al_{1.0}Ge_{0.2}Fe_2B_2$	2.928(6)/+0.07	11.038(2)/+0.08	2.873(8)/0.24	92.88	95; 5 wt% FeB	–
$Al_{0.9}Ge_{0.3}Fe_2B_2$	2.931(4)/+0.24	11.041(2)/+0.11	2.876(2)/0.35	93.07	83; 15 wt% FeB; 2 wt% Ge)	–
$Al_{1.1}Ga_{0.05}Ge_{0.05}Fe_2B_2$	2.928(9)/+0.07	11.038(4)/+0.08	2.872(7)/+0.21	92.88	100	2.03

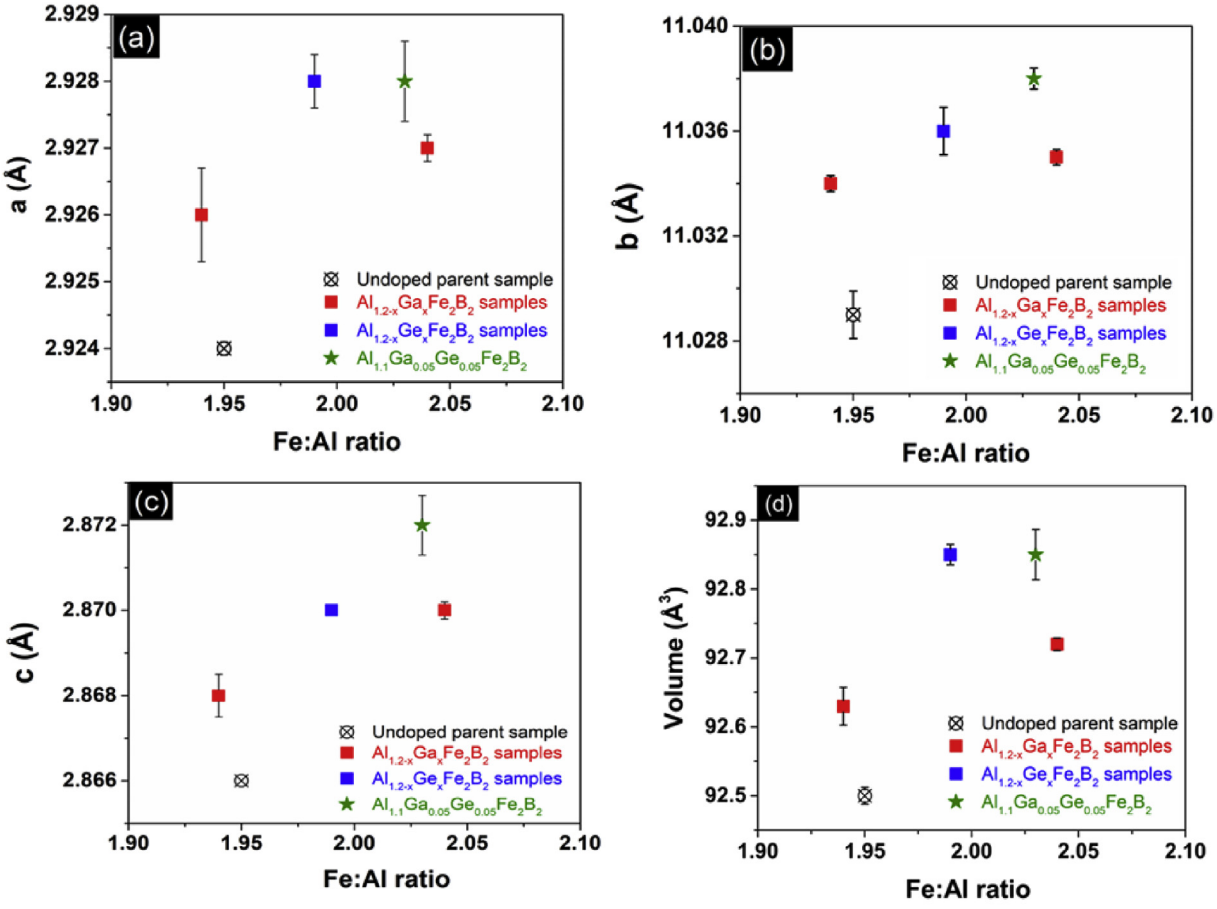

Fig. 6. Increase in unit cell volume and lattice parameters with increase in Fe:Al ratio in the 1-2-2 phase of annealed $Al_{1.2-x}M_xFe_2B_2$ (M = Ga and/or Ge; x < 0.1) samples.

$_x$(Ga,Ge)$_x$Fe$_2$B$_2$ samples systematically decreases with increased Ga and/or Ge concentration (Fig. 6), EDS shows negligible solubility for these elements in the $AlFe_2B_2$ lattice – an observation that suggests presence of a range of solid solution in $AlFe_2B_2$. It is hypothesized that addition of Ga and Ge alters the local equilibrium of $AlFe_2B_2$ to favor non-stoichiometric enrichment of Fe into the $AlFe_2B_2$ lattice. It is further proposed that these excess Fe atoms occupy the Al sites within the $AlFe_2B_2$ lattice in Fe-rich non-stoichiometric samples; this conclusion is supported by consideration of the covalent radii of constituent elements: the radius of Fe (125 pm) is closer to that of Al (118 pm) than to B (82 pm) [23], thus favoring antisite occupancy of Fe substituting for Al within the (*ac*) plane of the lattice. The measured increase from 1.96 to 2.04 in the Fe:Al atomic ratio with increased additions of Ga/Ge (Fig. 5) corroborates this hypothesis.

Antisite Fe occupancy on the lattice Al sites within the $AlFe_2B_2$ structure is anticipated to alter the interatomic bonding among the Fe, B and Al atoms. In this context, it is noted that the evolution of

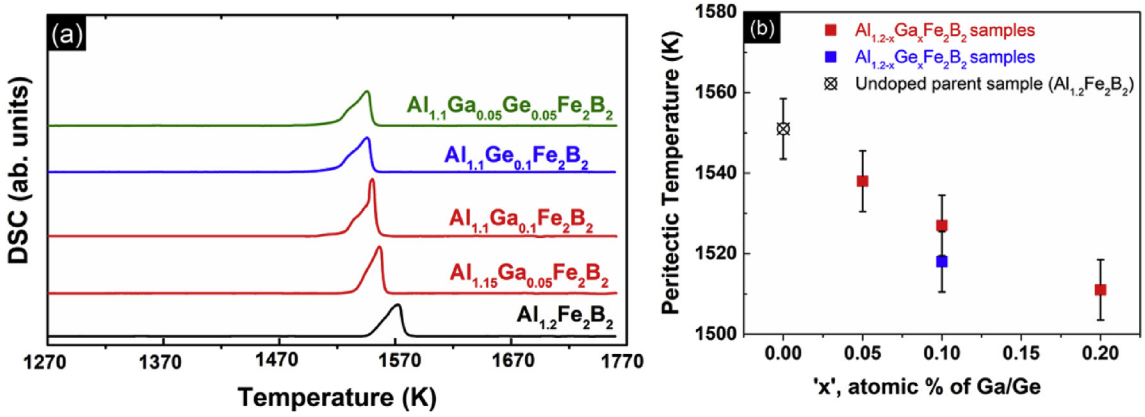

Fig. 7. Peritectic temperature as a function of 'x' content in samples of nominal composition $Al_{1.2-x}(Ga,Ge)_xFe_2B_2$ (x ≤ 0.1). Results indicate a decrease in peritectic temperature with increase in *x* content.

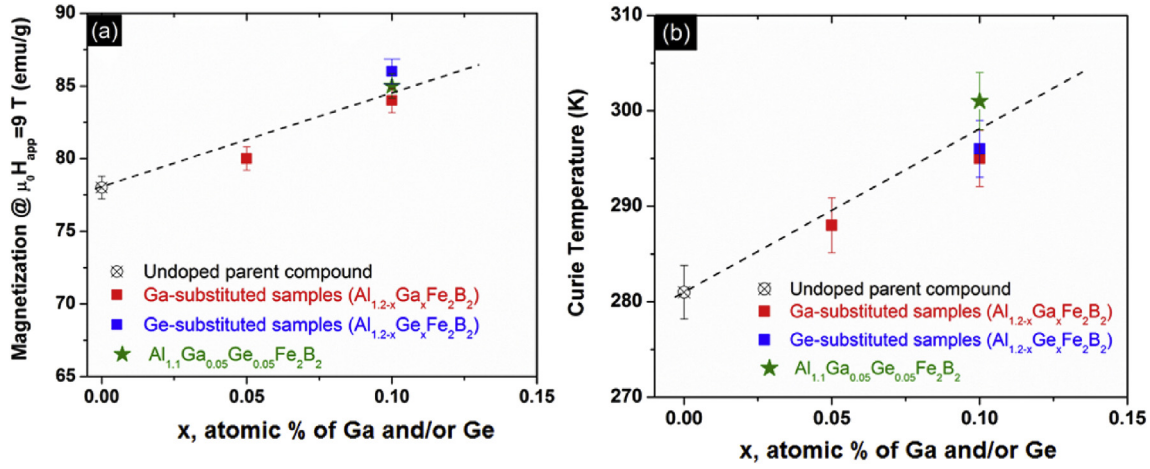

Fig. 8. Relationship between magnetic properties and the atomic % of Ga and Ge in samples of nominal chemical composition $Al_{1.2-x}(Ga,Ge)_xFe_2B_2$ ($x \leq 0.1$). Here, the dotted line merely serves as guide to eye.

Table 2
Magnetic properties of annealed samples of nominal composition. $Al_{1.2-x}M_xFe_2B_2$ (M = Ga and/or Ge, $0 < x \leq 0.30$).

General chemical composition	Curie temperature, T_C (K)	Saturation magnetization M_s at 50 K and $\mu_0 H = 9$ T(emu/g)	Effective magnetic moment per Fe atom (μ_B)[a]
$Al_{1.2}Fe_2B_2$	272	78	1.61
$Al_{1.15}Ga_{0.05}Fe_2B_2$	282	80	1.53
$Al_{1.1}Ga_{0.1}Fe_2B_2$	290	84	1.64
$Al_{1.0}Ga_{0.2}Fe_2B_2$	302	84	[b]
$Al_{1.1}Ge_{0.1}Fe_2B_2$	291	86	1.59
$Al_{1.0}Ge_{0.2}Fe_2B_2$	303	86	[b]
$Al_{0.9}Ge_{0.3}Fe_2B_2$	310	82	[b]
$Al_{1.1}Ga_{0.05}Ge_{0.05}Fe_2B_2$	294	85	1.62

[a] Effective magnetic moment (μ_B) for single-phase samples was determined experimentally from magnetothermal data.
[b] Could not be determined due to presence of secondary ferromagnetic phase above T_c.

lattice parameters with increased Ga/Ge substitution is anisotropic in character, with the *b*-axis expansion (bridging the stacks of Al and Fe_2B_2 slabs; see Fig. 1 for the crystal structure) considerably smaller than the corresponding *a*-axis and *c*-axis expansions that contain the Fe_2B_2 slabs, Fig. 3. This experimental observation is consistent with conclusions from theoretical studies that indicate bonding between the Fe—Fe and Fe-B atoms in the Fe_2B_2 chains within the *(ac)*-plane play a critical role in influencing the magnetic properties of this 1-2-2 system [15,20,24]. Recent computations performed by Ke et al. also demonstrate an anisotropic magnetoelastic effect in compositional variants of $AlFe_2B_2$ wherein the magnetization has a much stronger dependence on the *c*-lattice parameter than on the *a*- or *b*-lattice parameters [20].

These results indicate that the enhanced magnetofunctional response found in annealed samples of the $Al_{1.2-x}(Ga,Ge)_xFe_2B_2$ composition may be attributed to a combination of chemical

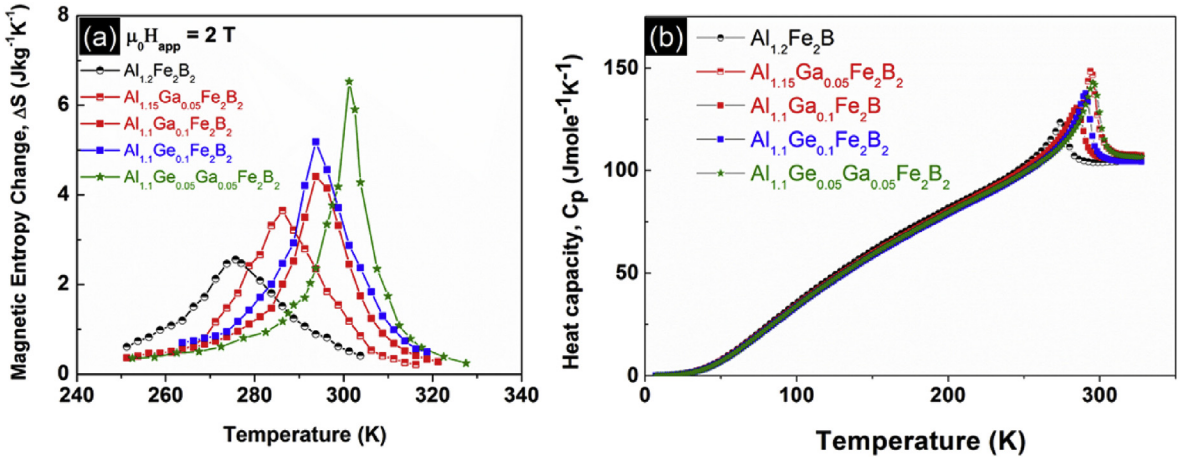

Fig. 9. (a) Magnetic entropy change curves of single phase samples of nominal composition, $Al_{1.2-x}(Ga,Ge)_xFe_2B_2$ ($x < 0.1$) at an applied magnetic field of $\mu_0 H_{app} = 2$T; (b) Temperature-dependence of the heat capacity of corresponding samples at zero applied magnetic field.

Table 3
Magnetocaloric properties of annealed samples of nominal composition. $Al_{1.2-x}M_xFe_2B_2$ (M = Ga and/or Ge, $0 < x \leq 0.1$).

General chemical composition	Magnetic entropy change at $\mu_0H_{app} = 2$ T, ΔS_{mag}^{peak} ($J \cdot kg^{-1}K^{-1}$ [1])	Adiabatic temperature change at $\mu_0H_{app} = 2$ T, ΔT^{ad} (K)	Working temperature range, δT_{FWHM} (K)	Heat Capacity at $\mu_0H_{app} = 0$ T, C_p (J/moleK)
$Al_{1.2}Fe_2B_2$	2.7	1	24	123
$Al_{1.15}Ga_{0.05}Fe_2B_2$	3.67	1.26	19	130
$Al_{1.1}Ga_{0.1}Fe_2B_2$	4.42	1.39	13	137
$Al_{1.1}Ge_{0.1}Fe_2B_2$	5.18	1.74	12	148
$Al_{1.1}Ga_{0.05}Ge_{0.05}Fe_2B_2$	6.51	2.19	11	144

Table 4
Magnetocaloric properties of $AlFe_2B_2$, Gd, MnFe(P,Si,Ge,As), and $La(FeSi)_{13}$-based alloys.[a]

	$AlFe_2B_2$-based alloys	Gd-based alloys	$La(Fe,Si)_{13}$-based alloys (including hydrides)	FeMn(P,Si, Ge, As)-based alloys
Raw material (cost, abundance)	¢¢	$$$$	$$	$
Ease of manufacturing	Moderate	Moderate	complex	Moderate
Environmental impact	Low	High	High	High
ΔS_{mag} ($J \cdot kg^{-1}K^{-1}$) at 2 T	Up to 6.5	6.1–14	8.4–24	11–31
ΔT_{ad} (K) at 2 T	Up to 2.2	6–7.5	3–7	3–6
Hysteresis (can be tailored)	Small	Moderate	Small	Small
Specific heat (J/moleK)	125–150	52–200	750–900	300
Corrosion susceptibility	Low (estimated)	Very high	High	Low
Mechanical integrity	High (estimated)	Low	Low	High

[a] Data taken from Refs. [5–9].

bonding and electronic effects arising from a hypothesized enrichment of Fe atoms on the Al sites within the (*ac*) plane of the $AlFe_2B_2$ lattice. In the course of this work, a particular sample of starting composition $Al_{1.1}Ge_{0.05}Ga_{0.05}Fe_2B_2$ has been confirmed to exhibit the largest magnetocaloric effect in any $AlFe_2B_2$-based sample reported to date, with $\Delta S_{mag}(2\,T) = 6.5\,J\,kg^{-1}K^{-1}$, $\Delta T_{ad}(2\,T)$ ~2.4 K. It is concluded that the magnetocaloric potential of the intermetallic boride $AlFe_2B_2$ is comparable to that of existing technologically relevant magnetocaloric materials, including $Gd_5Si_2Ge_2$, $La(FeSi)_{13}$ and MnFe(P,Si,Ge,As), Table 4 [4–6].

5. Conclusions

Changes in the structural, magnetic and magnetocaloric properties of $AlFe_2B_2$ due to the incorporation of very small amounts of Ga and Ge are reported. The magnetocaloric response of the $Al_{1.2-x}(Ga,Ge)_xFe_2B_2$ samples may be tuned over a temperature span of 50 K ranging from 260 K to 310 K by very small but systematic additions of Ga and/or Ge ($x \leq 0.3$). Relative to the unmodified parent alloy, a significant improvement in magnetocaloric response was noted in alloys of nominal starting chemical composition where $x \leq 0.1$. It is deduced that the additions of Ga and/or Ge to the precursor alloy composition alter the Al-Fe-B phase space such that less excess Al is required to obtain phase-pure samples and promote Fe solubility within the $AlFe_2B_2$ lattice. It is proposed that antisite occupancy of Fe on Al sites within the $AlFe_2B_2$ lattice alters the chemical bonding and electronic interactions between the Fe, B and Al constituents, particularly in the (*ac*)-plane. Consistent with theoretical reports, it is concluded that interatomic bonding between the Fe–Fe and Fe-B atoms within the Fe_2B_2 chains play a critical role in influencing the electronic structure and magnetic properties of $AlFe_2B_2$. The enhanced magnetocaloric response of the $Al_{1.2-x}(Ga,Ge)_xFe_2B_2$ system is thus attributed to an amalgamation of extrinsic (solidification pathway) and intrinsic (antisite occupancy) factors. These results provide fundamental and technological insight concerning predictive pathways for maximizing the magnetocaloric effect in the $AlFe_2B_2$ system.

Acknowledgement

We would like to thank Dr. E. M. Levin and Dr. R. T. Ott for useful discussions. This work was conducted at Northeastern University and Ames Laboratory under the auspices of the U.S. Department of Energy (DOE), Advanced Research Projects Agency – Energy (DE-AR00000754). Ames Laboratory is operated for the U.S. Department of Energy by Iowa State University under Contract No. DE-AC02-07CH11358.

Appendix A. Supplementary data

Supplementary data to this article can be found online at https://doi.org/10.1016/j.jallcom.2018.10.206.

References

[1] V. Franco, J.S. Blázquez, B. Ingale, A. Conde, The magnetocaloric effect and magnetic refrigeration near room temperature: materials and models, Annu. Rev. Mater. Res. 42 (1) (2012) 305–342.
[2] A. Kitanovski, U. Plaznik, U. Tomc, A. Poredoš, Present and future caloric refrigeration and heat-pump technologies, Int. J. Refrig. 57 (2015) 288–298.
[3] Z. Zhang, Y.J. Sun, E. Niu, L.H. Yang, J. Shen, F.X. Hu, J.R. Sun, B.G. Shen, Large magnetocaloric effects of R FeSi (R= Tb and Dy) compounds for magnetic refrigeration in nitrogen and natural gas liquefaction, Appl. Phys. Lett. 103 (20) (2013), 202412.
[4] J. Li, Y. Qu, J. Ren, W. Yuan, D. Shi, Magnetocaloric effect in magnetothermally-responsive nanocarriers for hyperthermia-triggered drug release, Nanotechnology 23 (50) (2012), 505706.
[5] R. Iglesias-Rey, A. Vieites-Prado, B. Argibay, F. Campos, M. Bañobre-López, T. Sobrino, J. Rivas, J. Castillo, Magnetocaloric effect for inducing hypothermia as new therapeutic strategy for stroke: a physical approach, J. Appl. Biomed. 15 (1) (2017) 33–38.
[6] S. Pandey, A. Quetz, A. Aryal, I. Dubenko, D. Mazumdar, S. Stadler, N. Ali, Thermosensitive Ni-based magnetic particles for self-controlled hyperthermia applications, J. Magn. Magn. Mater. 427 (2017) 200–205.
[7] R. Barua, F. Jimenez-Villacorta, L. Lewis, Towards tailoring the magnetocaloric response of FeRh-ternary compounds, J. Appl. Phys. 115 (2014), 17A903.
[8] E. Brück, O. Tegus, D.T. Cam Thanh, N.T. Trung, K.H.J. Buschow, A review on Mn based materials for magnetic refrigeration: structure and properties, Int. J. Refrig. 31 (2008) 763–770.
[9] J. Lyubina, O. Gutfleisch, M.D. Kuz'min, M. Richter, La (Fe, Si) 13-based magnetic refrigerants obtained by novel processing routes, J. Magn. Magn. Mater. 321 (21) (2009) 3571–3577.
[10] K.A. Gschneidner, V.K. Pecharsky, Magnetocaloric materials, Annu. Rev. Mater.

Res. 30 (2000) 387–429.
[11] R. Barua, X. Jiang, F. Jimenez-Villacorta, J.E. Shield, D. Heiman, L.H. Lewis, Tuning the magnetostructural phase transition in FeRh nanocomposites, J. Appl. Phys. 113 (2) (2013), 023910.
[12] I. Dubenko, N. Ali, S. Stadler, A. Zhukov, V. Zhukova, B. Hernando, V. Prida, V. Prudnikov, E. Gan'shina, A. Granovsky, Magnetic, magnetocaloric, magnetotransport, and magneto-optical properties of Ni–Mn–In-based heusler alloys: bulk, ribbons, and microwires, in: Novel Functional Magnetic Materials, Springer, Cham, 2016, pp. 41–82.
[13] X. Tan, P. Chai, C.M. Thompson, M. Shatruk, Magnetocaloric effect in AlFe2B2: toward magnetic refrigerants from earth-abundant elements, J. Am. Chem. 135 (2013) 9553–9557.
[14] Q. Du, G. Chen, W. Yang, Z. Song, M. Hua, H. Du, C. Wang, S. Liu, J. Han, Y. Zhang, J. Yang, Magnetic properties of $AlFe_2B_2$ and $CeMn_2Si_2$ synthesized by melt spinning of stoichiometric compositions, Jpn. J. Appl. Phys. 54 (2015), 053003.
[15] L.H. Lewis, R. Barua, B. Lejeune, Developing magnetofunctionality: coupled Structural and magnetic phase Transition in $AlFe_2B_2$, J. Alloys Compd. 650 (2015) 482.
[16] W. Jeitschko, The crystal structure of Fe_2AlB_2, Acta Crystallogr. 25 (1) (1969) 163.
[17] E.M. Levin, B.A. Jensen, R. Barua, R.W. McCallum, A. Howard, B. Lejeune, L.H. Lewis, M.J. Kramer, Effects of Al content and annealing on the phases formation, lattice parameters, and magnetization of $Al_xFe_2B_2$ ($x = 1.0, 1.1, 1.2$) alloys, Phys. Rev. Mater. 2 (2018), 034403.
[18] M. Cedervall, S. Andersson, T. Sarkar, E.K. DelczegCzirjak, L. Bergqvist, T.C. Hansen, P. Beran, P. Nordblad, M. Sahlberg, Magnetic structure of the magnetocaloric compound $AlFe_2B_2$, J. Alloys Compd. 664 (2016) 784.
[19] T.N. Lamichhane, L. Xiang, Q. Lin, T. Pandey, D.S. Parker, T. Kim, L. Zhou, Matthew J. Kramer, Sergey L. Bud'ko, P.C. Canfield, Magnetic properties of single crystalline itinerant ferromagnet $AlFe_2B_2$, Phys. Rev. Matl. 2 (2018), 084408.
[20] L. Ke, B.N. Harmon, M.J. Kramer, Electronic structure and magnetic properties in T_2AlB_2 (T= Fe, Mn, Cr, Co, and Ni) and their alloys, Phys. Rev. B 95 (10) (2017), 104427.
[21] R. Barua, B. Lejeune, L. Ke, G. Hadjipanayis, E. Levin, R.W. McCallum, M.J. Kramer, L.H. Lewis, Anisotropic magnetocaloric Response of layered $AlFe_2B_2$, J. Alloys Compd. 745 (2018) 505.
[22] P. Chai, S. a. Stoian, X. Tan, P. a. Dube, M. Shatruk, "Investigation of magnetic properties and electronic structure of layered-structure borides AlT_2B_2 (T=Fe, Mn, Cr) and $AlFe_{2-x}Mn_xB_2$, J. Solid State Chem. 222 (2015) 52.
[23] Q. Du, G. Chen, W. Yang, J. Wei, M. Hua, H. Du, C. Wang, S. Liu, J. Han, Y. Zhang, J. Yang, Magnetic frustration and magnetocaloric effect in AlFe2−xMnxB2 ($x = 0–0.5$) ribbons, J. Phys. D Appl. Phys. 48 (2015), 335001.
[24] K. Kadas, D. Iuşan, J. Hellsvik, J. Cedervall, P. Berastegui, M. Sahlberg, U. Jansson, O. Eriksson, AlM_2B_2 (M= Cr, Mn, Fe, Co, Ni): a group of nano-laminated materials, J. Phys. Condens. Matter 29 (2017) 155402.
[25] S. Hirt, F. Yuan, Y. Mozharivskyj, H. Hillebrecht, $AlFe_{2-x}Co_xB_2$ (x=0–0.30): T_c Tuning through Co Substitution for a promising magnetocaloric material Realized by spark plasma sintering, Inorg. Chem. 55 (19) (2016) 9677.
[26] Scott A. Speakman, Introduction to PANalytical X'Pert HighScore Plus V3. 0, MIT Center for Materials Science and Engineering, 2012.